RSC Advances

This is an *Accepted Manuscript*, which has been through the Royal Society of Chemistry peer review process and has been accepted for publication.

Accepted Manuscripts are published online shortly after acceptance, before technical editing, formatting and proof reading. Using this free service, authors can make their results available to the community, in citable form, before we publish the edited article. This *Accepted Manuscript* will be replaced by the edited, formatted and paginated article as soon as this is available.

You can find more information about *Accepted Manuscripts* in the Information for Authors.

Please note that technical editing may introduce minor changes to the text and/or graphics, which may alter content. The journal's standard Terms & Conditions and the Ethical guidelines still apply. In no event shall the Royal Society of Chemistry be held responsible for any errors or omissions in this *Accepted Manuscript* or any consequences arising from the use of any information it contains.

ROYAL SOCIETY OF CHEMISTRY

www.rsc.org/advances

One-pot, template-free synthesis of hydrophobic single-crystalline $La(OH)_3$ nanowires with tunable size and their d^0 ferromagnetic properties

Juan Feng[a, b], Xinghua Li[a, *], Mingzi Wang[a], Xinliang Zheng[a], Jintao Bai[a, c], Li Wang[b], Yong Peng[b, *]

[a] School of Physics, Northwest University, Xi'an 730000

[b] Key Laboratory of Magnetism and Magnetic Materials of Ministry of Education, School of Physical Science and Technology, Lanzhou University, Lanzhou 730000, China

[c] Institute of Photonics and Photo-Technology, Provincial Key Laboratory of Photoelectronic Technology, Northwest University, Xi'an 730000, China

* Corresponding authors: Xinghua Li (lixinghua04@gmail.com) and Yong Peng (pengy@lzu.edu.cn)

Abstract

Hydrophobic single-crystalline $La(OH)_3$ nanowires with tunable size have been successfully fabricated by a facile one-pot liquid-solid-solution (LSS) assisted hydrothermal method without any template and their morphology, chemistry and crystal structure were characterized at the nanoscale. Their average diameter and length strongly depend on the reaction time and the selection of solvents, which is due

RSC Advances Accepted Manuscript

to the Ostwald ripening and oriented attachment mechanisms. XRD pattern and SAED analysis of numerous nanowires show that the $La(OH)_3$ nanowires have a pure hexagonal structure without any impurity. TEM image and HAADF-STEM element mapping analysis indicate that the $La(OH)_3$ nanowires have a uniform size, smooth surface and pure chemical phase. HRTEM image and CBED pattern of individual $La(OH)_3$ nanowires suggest that each nanowires is single crystalline. Magnetic measurements reveal that the $La(OH)_3$ nanowires show a d^0 room-temperature ferromagnetic behavior. This study highlights the basic morphological, chemical and structural information for $La(OH)_3$ nanowires, which is critical for their applications in nanodevices and nanoelectronics.

Keywords: $La(OH)_3$, nanowires, single-crystalline, hydrothermal, magnetic properties.

1. Introduction

Since the discovery of carbon nanotubes in 1991,[1] the design and synthesis of one-dimensional (1D) nanostructures has been an exciting, fascinating and rapidly expanding research field in nanoscience and nanotechnology over the past few years, owning to their outstanding magnetic, electrical and optical properties along with unique high-aspect-ratio effect.[2-10] These remarkable properties are significant not only from a fundamental point in mesoscopic physics, such as quantized conduction, spin transport, electron-phonon and electron-electron effect which are different from their corresponding bulk and nanoparticles,[11,12] but also for their potential applications in nanodevice generation as active components.[13,14] Nowadays, many groundbreaking

RSC Advances Accepted Manuscript

efforts have been made on the fabrication of 1D nanostructural materials.[9,15-20] However, it is still a big challenge to precisely control the sizes, purity, compositions and crystal structures of 1D nanomaterials in nanoscale in the absence of catalysts and templates.[20, 21]

As a kind of the most fascinating functional nanomaterials, rare earth compounds have been extensively investigated in both the fundamental science and technological applications owing to their special physical and chemical characteristic originating from the electron transition in 4f shell.[22-27] Among them, nanostructured lanthanum hydroxides ($La(OH)_3$) have been widely applied in fields of catalyst,[28] superconductors,[29] optical coatings,[30] exhaust-gas convectors,[31] hydrogen storage materials[32] and high dielectric constant gate dielectrics.[33] As we know, the advanced functions and applications of nanostructures strongly depend on their chemical and physical properties, which are greatly influenced by not only the crystal structures and chemical compositions but also the shape, size and dimensionality of the nanostructures. Therefore, when rare earth hydroxides are prepared in the form of 1D nanostructures, they are proposed to be novel functionalized materials resulting from the unique shape and quantum confinement effects. Besides, the 1D rare earth hydroxides can be used for the construction of nanoelectronics and nanodevices, owing to that the 1D morphology could be employed as nanoscale building blocks to make the electrical measurement with two terminals easier.[10,34] Up to now, several strategies have been explored for the fabrication of $La(OH)_3$ nanowires, including sol–gel,[35] hydrothermal,[36] solvothermal,[37] template-assisted routes,[38]

RSC Advances Accepted Manuscript

microwave-assisted routes[39] and composite-hydroxide-mediated method.[40] However, the synthesis routes are in need of either the preparation of La-based precursors or templates was needed. Recently, Li and his co-workers developed a facile liquid-solid-solution (LSS) phase transfer synthetic strategy, using which a variety of nearly monodisperse and hydrophobic nanocrystals, including noble metals, semiconductors, ferrites, rare earth fluorides and so on, have been synthesized.[41,42] We also contributed an improvement to this strategy for the fabrication $CoFe_2O_4$ and $NiFe_2O_4$ nanocrystals.[43,44] In comparison with the other chemical methods, the LSS phase transfer synthetic strategy shows several advantages, including great chemical flexibility, synthetic tenability, inherent simplicity, cleanliness, low cost and the capability of large-scale production. However, to our best knowledge, no paper has been reported on the synthesis of hydrophobic rare earth oxide nanostructures, especially using this LSS-assisted phase transfer strategy.

In this paper, we report the fabrication of hydrophobic single-crystalline $La(OH)_3$ nanowires with tunable size by a LSS-assisted hydrothermal route for the first time. The influences of reaction time and solvent selections on the formation of the $La(OH)_3$ nanowires are investigated. We also devote a nanoscale characterization of individual $La(OH)_3$ nanowires. The magnetic properties of the $La(OH)_3$ nanowires were also investigated. It is believed that this work is significant for the fundamental research and applications of rare earth compounds.

2. Experimental section

2.1 Materials

RSC Advances Accepted Manuscript

All chemical reagents used in this work were directly used as received and without any further purification. Lanthanum chloride heptahydride ($LaCl_3 \cdot 7H_2O$, AR 99.5%) was purchased from the Recovery Fine Chemical Industry Research Institute (Tianjin, China). Sodium oleate ($C_{18}H_{33}NaO_2$, CP) was purchased from Guoyao Chemical Company (Shanghai, China). Sodium hydroxide (NaOH, 98%) and Oleic acid ($C_{18}H_{34}O_2$, 90%) were purchased from Alfa Aesar. Ethanol alcohol (C_2H_6O, analytical grade) was purchased from Rionlon BoHua Pharmaceutical and Chemical Limited Company (Tianjin, China). Deionized water used through the experiment was obtained by means of a water-purification system.

2.2 Synthesis of $La(OH)_3$ nanowires

In a typical process, 2 mmol $LaCl_3 \cdot 7H_2O$ were dissolved in the solvent composed of 20 ml water and 10 ml ethanol alcohol. Then 6 mmol sodium oleate and 5 ml oleic acid were introduced and vigorously stirred at room temperature for 2 h to obtain a homogenous solution. After that, 36 mmol NaOH was added and strongly stirred for another 0.5 h. The prepared solution was transferred into an 80-mL-capacity stainless Teflon-lined autoclave, which was sealed and maintained at 180 ^oC for 20 h and then naturally cooled to room temperature. The products were collected by a centrifugation, washed with hexane several times, and dried at 60 ^oC for 24 h.

2.3 Characterizations

The morphology, chemistry and crystal structure of individual $La(OH)_3$ nanowires were analysed at the nanoscale using a field-emission scanning electron microscopy (FESEM, S-4800, Hitachi), high-resolution transmission electron microscope

RSC Advances Accepted Manuscript

(TEM, TecnaiTM G^2 F30, FEI) equipped with energy-dispersive X-ray spectrum (EDAX, AMETEK), high angle annular dark field and scanning transmission electron microscopy (HAADF-STEM), an X-ray diffraction instrument (XRD, Philips X'pert Pro MPD, Cu Kα radiation, Netherlands), Fourier transform infrared (FTIR) spectrometer (170SX, Nicolet). $La(OH)_3$ nanowires dispersed in hexane were dispersed on holey carbon film coated Cu grids for TEM measurements. Magnetic properties of the $La(OH)_3$ nanowires were measured by an vibrating sample magnetometer (VSM, Microsence VSM ev9). The Ce impurity is measured by inductively coupled plasma emission spectrometer (ICP-ES) (IRIS Intrepid ER/S, Thermo Elemental) and Quantum Design MPMS magnetometer based on superconducting quantum interference device (SQUID) (MPMS-XL-7, Quantum Design). Electron spin resonance (ESR) spectrum was recorded in X-band (8.984 GHz) by a JES-FA300 spectrometer (JEOL).

3. Results and Discussion

3.1 Crystal structure, morphology, chemical component and magnetic properties of the $La(OH)_3$ nanowires

The phase crystal structure of the $La(OH)_3$ nanowires was characterized by XRD technique, as shown in Fig. 1. The positions and relative intensities of all the peaks could be indexed to a pure hexagonal structure (space group: P 63/m (176)) of $La(OH)_3$ with lattice constants of a = b = 6.529 Å and c = 3.859 Å, which is in accordance with the standard JCPDS card No.36-1481. No additional diffraction peaks of other impurity phases are observed. In addition, it is clearly seen that the

RSC Advances Accepted Manuscript

diffraction peaks of the $La(OH)_3$ nanowires obtained in this work show broadening effect, which is due to the small crystalline structures.

The morphologies of $La(OH)_3$ nanowires prepared in this work were characterized by SEM and TEM. Fig. 2 (a) shows a representative SEM image of bundles of $La(OH)_3$ nanowires. Continuous structure and virtually uniform diameter can be seen in each nanowires. The nanowires are randomly distributed and closely interwoven, forming net structures. Fig. 2 (b) shows a bright field (BF) TEM image of tens of dispersed $La(OH)_3$ nanowires, which provides a further insight into their morphology. It is clearly seen that individual nanowires have smooth surface and uniform diameter. The average diameter is about 15 nm and the length is approximately 300 nm.

To further investigate the spatial shape of the nanomaterials, HAADF-STEM technology was adopted to analyze the $La(OH)_3$ nanowires due to its better depth of field and spatial resolution in comparison with the SEM and TEM. Fig. 2 (c) shows a representative low-magnified HAADF-STEM image of the $La(OH)_3$ nanowires. It is clear seen that the $La(OH)_3$ nanostructures show wire-like shape with nearly monodispersed diameter, which is accordant with the SEM and TEM results. The HAADF-STEM image is also called *Z*-contrast image, which strongly depends on the atomic number (Z) and thickness (d) of the samples. The $La(OH)_3$ nanowires show smooth surface and no defects are observed, revealing that the sample have a good qualify. In addition, uniform contrast can be seen for each nanowire indicating that the $La(OH)_3$ nanowires have a pure chemical phase.

Fig. 2 (d) shows a representative selected area electron diffraction (SAED) pattern

RSC Advances Accepted Manuscript

of a bundle of $La(OH)_3$ nanowires marked by red circle in Fig. 2 (b). Several distinguishable and bright diffraction rings can be seen, indicating the high crystalline feature of the $La(OH)_3$ nanowires. The diffraction rings can be indexed to the (200), (102), and (310) lattice planes, suggesting the formation of hexagonal phase of $La(OH)_3$, which is in accordance with the XRD data. Detailed analysis of HRTEM image was further used to determine the crystalline structure of $La(OH)_3$ nanowires. Fig. 2 (e) shows the lattice-resolution HRTEM image of the local area B marked by blue box on the single nanowire in Fig. 2 (b). The clear lattice fringes suggest the high crystalline nature of the $La(OH)_3$ nanowires. The measured interplanar distance is about 0.3188 nm, which can be assigned to the (101) plane of hexagonal $La(OH)_3$. Fig. 2 (f) displays the converged beam electron diffraction (CBED) pattern of the area B marked by green circle on the single nanowire in Fig. 2 (b). The result shows a single crystalline hexagonal structure with <0001> orientation. Fig. 2 (g) shows the structure model of the hexagonal $La(OH)_3$, indicating a highly anisotropic structure. The view of this model along *c*-axis direction is shown in Fig. 2 (h). It is believed that the anisotropic growth of $La(OH)_3$ nanowires is governed by the inherent crystal structure and their chemical potential in the solution.[9] More HRTEM and CBED results prove that individual $La(OH)_3$ nanowires have a single crystalline nanostructure.

The chemical element distributions of $La(OH)_3$ nanowires were further studied by HAADF-STEM and EDX elemental mapping analysis techniques. The typical HAADF-STEM image of a single $La(OH)_3$ nanowire is shown in Fig. 3 (a). Smooth surface and no defects are observed. Fig. 3 (b) displays the EDX spectrum of the

RSC Advances Accepted Manuscript

$La(OH)_3$ nanowires. The spectrum demonstrates the existence of lanthanum (La) and oxygen (O) in the samples, while hydrogen (H) cannot be detected by EDX. This result is in coincident with the XRD data. The carbon (C) and copper (Cu) peaks in the EDX spectrum is due to the carbon-coated copper grids, which has been demonstrated by the EDX spectrum of an empty carbon-coated copper grid. Fig. 3 (c) and (d) show the corresponding EDX mappings of La (K_a, 4.65 keV) and O (K_a, 0.52 keV), respectively. It is clear that the elements La and O are evenly distributed throughout the whole nanowire, revealing a uniform chemical phase. This result is in good agreement with the above TEM observations.

FTIR spectroscopy was employed to analyze the chemical bonding on the surface of the $La(OH)_3$ nanowires, as shown in Fig. 4. The sharp peaks at 2925 and 2855 cm^{-1} are assigned to the asymmetric and symmetric stretching modes of the long CH_2 chains, respectively. The peaks at 1562 and 1447 cm^{-1} are attributed to the asymmetric and symmetric COO^-, respectively. The sharp peak at 3612 cm^{-1} is associated with the vibration of O-H bonds in the hydroxide. The peak at 646 cm^{-1} is attributed to the stretching vibration of La-O bonds. This result suggests the formation of $La(OH)_3$, which is accordant with the XRD and EDX results. In addition, the FTIR spectrum confirms that the surface of the $La(OH)_3$ nanowires prepared in this work is decorated by oleic acid, which can afford steric repulsive force to balance the gravity of the nanowires. Therefore, the $La(OH)_3$ nanowires can be easily dispersed in the nonpolar solvents without agglomeration as shown in the inset of Fig. 4.

Fig. 5 shows the magnetization versus magnetic field (M-H) curve of the $La(OH)_3$

RSC Advances Accepted Manuscript

nanowires measured by VSM at room temperature, in which the paramagnetic and anti-ferromagnetic signals of the samples have been subtracted. The VSM equipment is one of the most powerful tools to measure the net magnetization of samples, which has a resolution of 10^{-6} emu.[45] It is clearly seen that the *M*-*H* curve reveals an S-shape. The saturated magnetization value is about 0.047 emu g^{-1}. A distinct hysteresis loop with coercivity (H_c) of 183 Oe and remanence magnetization (M_r) of 0.0065 emu g^{-1} can be obtained in the magnification of the central part of the curve as shown in the right-below inset. These results indicate that the $La(OH)_3$ nanowires prepared in this work have room temperature ferromagnetic (RTFM) characteristic, while the corresponding bulk $La(OH)_3$ is well known as an antiferromagnetic material.

In order to investigate the physical origin of RTFM characteristic of the $La(OH)_3$ nanowires prepared in this work, the zero-field-cooled (ZFC) and field-cooled (FC) curves of the $La(OH)_3$ nanowires are measured using the SQUID equipment in the temperature range from 10 to 300 K under an applied magnetic field of 100 Oe, as shown in Fig. 6. In is clearly seen that no blocking temperature (T_B) is obtained, suggesting that there is no contamination of ferromagnetic clusters formed in the sample.[46] This result indicates that the observed RTFM characteristic of the $La(OH)_3$ nanowires should be originated from their intrinsic nature. Moreover, the FC curve is obviously deviated from the ZFC curve in the whole measured temperature range, indicating that the Curie temperature (T_C) of the sample is above 300 K. This result suggests that the $La(OH)_3$ nanowires have clear RTFM characteristic, which is accordant with the VSM data. The temperature dependence of magnetization (*M*-*T*)

RSC Advances Accepted Manuscript

curve of the $La(OH)_3$ nanowires were analyzed under an external magnetic field of 1000 Oe from 10 to 300 K, as shown in Fig. 7. The magnetization of the $La(OH)_3$ nanowires decreases rapidly from 10 to 50 K, and then slowly reduced with the increase of temperature. The *M-T* curve doesn't occur the first derivative, and the magnetization is non-zero in the whole measured temperature range. These results indicate that T_C of the sample is above 300 K, which is consistent with the ZFC-FC result.

To further understand the specific d^0 RTFM characteristic of the $La(OH)_3$ nanowires, ESR technology was adopted to investigate the microscopic magnetic information of the samples. Fig. 8 shows the ESR spectrum of the $La(OH)_3$ nanowires measured at room temperature. The ESR spectrum shows a broad resonance band with a resonance field (H_R) at about 277 mT. This is quite different with the paramagnetic materials which have a H_R value of 321 mT.[23] According to the magnetic resonance theory, the effective *g* factor (g_{eff}) can be obtained by the following equations:[23]

$$g_{eff} = (h\nu_m)/(\mu_B H_R)$$

where *h* is the plank constant, ν_m is the frequency of the applied microwave field, μ_B is the Bohr magnetron and H_R is the resonance magnetic field. The calculated g_{eff} value of the $La(OH)_3$ nanowires is about 2.3204, which is far away from that of the free electron (g_{eff} = 2.0023). These ESR results further demonstrate that the $La(OH)_3$ nanowires represent d^0 RTFM characteristic, which is consistent with the VSM results.

RSC Advances Accepted Manuscript

It is well known that the paramagnetic Ce ion impurity is frequently occurs in La-based compounds, which may also cause ferromagnetic behavior. To check the content of Ce impurity in the sample, inductively coupled plasma atomic emission spectroscopy (ICP-AES) was employed, displaying a 1.3:98.7 molar ratio of Ce and La. The Ce element is usually existed as ceria (CeO_2) in the hydroxide or oxide. Therefore, the Ce impurity presented in the $La(OH)_3$ nanowires should be performed as CeO_2. The M_s value of CeO_2 nanostructures is reported to be only several memu g^{-1},[51-54] while the M_s value of the $La(OH)_3$ nanowires prepared in this work is 0.047 emu g^{-1}. It is clear that the influence of Ce impurity on the magnetization of $La(OH)_3$ nanowires can be ignored.

All the results above suggest that the measured RTFM charactertistic undoubtedly reveal the intrinsic nature of the $La(OH)_3$ nanowires prepared in this work. Generally, the RTFM characteristic of rare earth-based nanostructures is probably due to the permanent magnetic moment per rare earth ion which has the existence of unpaired electrons.[23,51] However, the La^{3+} performs a stable electron structure like xenon (Xe) without any unpaired electrons. Therefore, the specific d^0 RTFM behavior of the $La(OH)_3$ nanowires is possibly owing to the point defects originated from the size effect, which can restrict the compensating charges in molecular orbitals and form a local magnetic moment.[52-54]

3.2 Morphologies influenced by reaction time and solvent selections

In order to elucidate the growth mechanism of the $La(OH)_3$ nanowires, the morphologies and crystal structures of the prepared $La(OH)_3$ nanowires were studied

RSC Advances Accepted Manuscript

by changing the experimental parameters, such as reaction temperature, reaction time, concentration of NaOH and selections of starting solvents. It is find that the reaction temperature and concentration of NaOH showed little impact on the morphologies of the $La(OH)_3$ nanowires. The main factors impacted on the morphologies are reaction time and the selections of solvents, which have been discussed in detail as follows.

Fig. 9 shows the TEM images of the $La(OH)_3$ nanowires synthesized at 180 ^oC with a molar ratio of H_2O to ethanol of 2:1 for 5, 10, 20, and 40 h. respectively. When the reaction time was reduced to 5 h, the products are mixture of tiny nanoparticles and nanorods as shown in Fig. 9 (a). The nanoparticles are about 5 nm in size, and the nanorods are about 8 nm in diameter and 70 nm in length. When the reaction time was prolonged to 10 h, the length of nanowires increases to approximate 250 nm and the diameter is about 13 nm (Fig. 9 (b)). When the reaction time lasted for 20 h, the average length is about 300 nm and the diameter is about 15 nm (Fig. 9 (c)). However, their sizes are more uniform and surface more smooth. While the reaction time was extended to 40 h, the diameter of the $La(OH)_3$ nanowires is up to 18 nm and length is about 7 nm, and individual nanowires are twisted together because of their long length (Fig. 9 (d)). These results suggest that the reaction time shows significant influence on the length of the $La(OH)_3$ nanowires but little impact on the diameter.

Fig. 10 shows the TEM images of the $La(OH)_3$ nanowires synthesized at 180 ^oC for 20 h with different volume of H_2O to ethanol. Using only H_2O as the solvent, $La(OH)_3$ nanowires with diameters of 4.5 nm and lengths of 40 nm were obtained (Figure 10 (a)). When the solvent become the mixture of 10 ml of H_2O and 20 ml of

RSC Advances Accepted Manuscript

ethanol, the average nanowire diameter is about 15 nm and lengths is about 300 nm (Figure 10 (b)). When the mixture solvent consists of 20 ml of H_2O and 10 ml of ethanol, the diameters of nanowires became uneven, some are about 12 nm, but the others about 35 nm (Figure 10 (c)). While pure ethanol was only used as the solvent, the size of the $La(OH)_3$ nanowires become uniform with about 180 nm diameter and 2.7 μm length (Figure 10 (d)). This result shows that the solvent selections strongly impact on not only the diameter but also the length of the $La(OH)_3$ nanowires.

Based on the above experimental results, the formation mechanism of the $La(OH)_3$ nanowires at different conditions are schematically illustrated in Fig. 11. By changing the reaction time, the formation of $La(OH)_3$ nanowires experiences two dominant growth mechanisms, including Ostwald ripening and oriented attachment. When the reaction time is less than 5 h, the tiny $La(OH)_3$ nanoparticles formed based on the Ostwald ripening mechanism.[54] Besides, the $La(OH)_3$ nanorods with low length-diameter ratio formed at 5 h was possibly due to the partial fusion of some tiny nanoparticles. By prolonging the reaction time, the length-diameter ratio of the nanowires was obviously enhanced, which was due to the aggregation of nanoparticles into nanowires based on the oriented attachment.[54] However, when the polarity of the solvent decreases (decreasing the volume ratio of water/ ethanol), more oleic acid might surround around the $La(OH)_3$ precursor. During the hydrothermal process, Ostwald ripening and oriented attachment mechanisms happened at the same time, leading to the formation of nanowires with larger diameter and length.

4. Conclusion

RSC Advances Accepted Manuscript

In summary, we reported a facile, efficient and rapid one-pot LSS-assisted hydrothermal method for the fabrication of 1D $La(OH)_3$ nanowires with tunable size without any template. The average lengths and diameter of $La(OH)_3$ nanowires can by tuned by facilely change the experimental parameters such as reaction time and solvents. Besides, the formation mechanisms of the nanowires are possibly Ostwald ripening and oriented attachment mechanisms. Detailed structural characterization revealed that individual $La(OH)_3$ nanowires are single crystalline hexagonal structure with <0001> orientation. The surface of the $La(OH)_3$ nanowires is capped by oleic acid, leading to a hydrophobic characteristic. Our study also shows that $La(OH)_3$ nanowires show d^0 room temperature ferromagnetism. This study highlights the basic morphological, chemical, structural information and magnetic properties for $La(OH)_3$ nanowires, which is believed to be critical for the rare earth compounds in fields of fundamental research and potential applications in nanodevices and nanoelectronics.

Acknowledgments

We thank the support from the grants from the National Natural Science Foundation of China (No. 61177059), Introduction Talent Project of Northwest University (pr13100), the Natural Science Foundation of Shannxi Province, China (2014JQ1040), the Research Project of Educational Department of Shaanxi Provence, China (14JK1727) and the Scientific Research Foundation of Northwest University (13NW13).

References

[1] S. Iijima, *Nature*, 1991, **354**, 56.

RSC Advances Accepted Manuscript

[2] S. Mann, *Nat. Mater.*, 2009, **8**, 781.

[3] Y. N. Xia, P. D. Yang, Y. G. Sun, Y. Y. Wu, B. Mayers, B. Gates, Y. D. Yin, F. Kim, H. Q. Yan, *Adv. Mater.*, 2003, **15**, 353.

[4] P. M. Rørvik, T. Grande, M. A. Einarsrud, *Adv. Mater.*, 2011, **23**, 4007.

[5] C. C. Lee, C. Grenier, E. W. Meijer, A. P. H. J. Schenning, *Chem. Soc. Rev.*, 2009, **38**, 671.

[6] Z. G. Yin, Q. D. Zheng, *Adv. Energy Mater.*, 2012, **2**, 179.

[7] M. Hasegawa, M. Iyoda, *Chem. Soc. Rev.*, 2010, **39**, 2420.

[8] A. N. Aleshin, *Adv. Mater.*, 2006, **18**, 17.

[9] M. I .B. Utama, J. Zhang, R. Chen, X. L. Xu, D. H. Li, H. D. Sun, Q. H. Xiong, *Nanoscale*, 2012, **4**, 1422.

[10] R. S. Devan, R. A. Patil, J. H. Lin, Y. R. Ma, *Adv. Funct. Mater.*, 2012, **22**, 3326.

[11] D. R. Bowler, *J. Phys.: Condens. Matter.*, 2004, **16**, R721.

[12] F. Zaldívar, J. L. D. Río-Correa, E. García-Martínez, M. Fernández-Guasti, Am. J. Phys., 2011, 79, 1060.

[13] B. Su, Y. C. Wu, L. Jiang, *Chem. Soc. Rev.*, 2012, **41**, 7832.

[14] C. W. Cheng, H. J. Fan, *Nano Today*, 2012, **7**, 327.

[15] T. R. Kline, M. Tian, J. Wang, A. Sen, M. W. H. Chan, T. E. Mallouk, *Inorg. Chem.*, 2006, **45**, 7555.

[16] L. Li, T. Zhai, H. Zeng, X. Fang, Y. Bando, D. Golberg, *J. Mater. Chem.*, 2011, **21**, 40.

[17] E. Comini, C. Baratto, G. Faglia, M. Ferroni, A. Vomiero, G. Sberveglieri, *Prog.*

RSC Advances Accepted Manuscript

Mater. Sci., 2009, **54**, 1.

[18] C. Bae, H. Yoo, S. Kim, K. Lee, J. Kim, M. M. Sung, H. Shin, *Chem. Mater.*, 2008, **20**, 756.

[19] N. Wang, Y. Cai, R. Q. Zhang, *Mater. Sci. Eng. R*, 2008, **60**, 1.

[20] X. Wang, Y. D. Li, *Inorg. Chem.*, 2006, **45**, 7522.

[21] T. Xia, J. Wang, N. Lin, H. Zhao, L. Huo, G. Mountrichas, *RSC Adv.*, 2011, **1**, 440.

[22] G. F. Wang, Q. Peng, Y. D. Li, *Acc. Chem. Res.*, 2011, **44**, 322.

[23] X. H. Li, X. Deng, H. Zhu, J. Feng, Y. Peng, J. T. Bai, X. L. Zheng, H. B. Fan, M. Z. Wang, H. W. Chen, *Chem. Asian J.*, 2014, **9**, 584.

[24] C. W. Sun, H. Li, L. Q. Chen, *Energy Environ. Sci.*, 2012, **5**, 8475.

[25] A. Jha, B. Richards, G. Jose, T. T. Fernandez, P. Joshi, X. Jiang, J. Lousteau, *Prog. Mater. Sci.*, 2012, **57**, 1426.

[26] A. Gnach, A. Bednarkiewicz, *Nano Today*, 2012, **7**, 532.

[27] M. Z. Wang, X. Deng, J. Feng, B. Z. Yu, H. Zhu, X. H. Li, X. L. Zheng, J. T. Bai, Y. Peng, *J. Alloy. Compd.*, 2015, **619**, 681.

[28] X. Ma, H. Zhang, Y. Ji, J. Xu, D. Yang, *Mater. Lett.*, 2004, **58**, 1180.

[29] A. Neumann, D. Walter, *Thermochim. Acta*, 2006, **445**, 200.

[30] S. J. Jo, J. S. Ha, N. K. Park, D. K. Kang, B. H. Kim, *Thin Solid Films*, 2006, **513**, 253.

[31] G. A. H. Mekhemer, B. A. A. Balboul, *Colloids Surf. A: Physicochem. Eng. Aspects*, 2001, **181**, 19.

[32] B. Hou, Y. Xu, D. Wu, Y. Sun, *J. Mater. Sci.*, 2007, **42**, 1397.

RSC Advances Accepted Manuscript

[33] J. H. Jun, D. J. Choi, *Thin Solid Films*, 2006, **504**, 205.

[34] G. Wang, Z. D. Wang, Y. X. Zhang, G. T. Fei, L. D. Zhang, *Nanotech.*, 2004, **15**, 1307.

[35] I. Djerdj, G. Garnweitner, D. S. Su, M. Niederberger, *J. Solid State Chem.*, 2007, **180**, 2154.

[36] X. Wang, Y. Li, *Chem. Eur. J.*, 2003, **9**, 5627.

[37] B. Tang, J. Ge, C. Wu, L. Zhuo, J. Niu, Z. Chen, Z. Shi, Y. Dong, *Nanotech.*, 2004, **15**, 1273.

[38] F. Bouyer, N. Sanson, M. Destarac, C. Gérardin, *N. J. Chem.*, 2006, **30**, 399.

[39] H. L. Zhu, D. R. Yang, H. Yang, L. M. Zhu, D. S. Li, D. L. Jin, K. H. Yao, *J. Nanopart. Res.*, 2008, **10**, 307.

[40] C. Hu, H. Liu, W. Dong, Y.Zhang, G. Bao, C. Lao, and Z. Wang, *Adv. Mater.*, 2007, **19**, 470.

[41] X. Wang, J. Zhuang, Q. Peng, Y. D. Li, *Nature*, **437**, 121.

[42] X. Liang, X. Wang, J. Zhuang, Y. T. Chen, D. S. Wang, Y. D. Li, *Adv. Funct. Mater.*, 2006, **16**, 1805.

[43] X. H. Li, C. L. Xu, X. H. Han, L. Qiao, T. Wang, F. S. Li, *Nanoscale Res. Lett.*, 2010, **5**, 1039.

[44] X. H. Li, G. G. Tan, W. Chen, B. F. Zhou, D. S. Xue, Y. Peng, F. S. Li, N. J. Mellors, *J. Nanopart. Res.*, 2012, **14**, 751.

[45] S. Foner, *Rev. Sci. Instrum.*, 1959, **30**, 548-557.

[46] J. Zhang, D. Q. Gao, G. J. Yang, J. L. Zhang, Z. H. Shi, Z. H. Zhang, Z. H. Zhu, D.

RSC Advances Accepted Manuscript

S. Xue, Nanoscale Res. Lett., 2011, 6, 587.

[47] A. Sundaresan, R. Bhargavi, N. Rangarajan, U. Siddesh, C. N. R. Rao, *Phys. Rev. B*, 2006, **74**, 161306.

[48] M. Y. Ge, H. Wang, E. Z. Liu, J. F. Liu, J. Z. Jiang, Y. K. Li, Z. A. Xu, H. Y. Li, *Appl. Phys. Lett.*, 2008, **93**, 062505.

[49] M. J. Li, S. H. Ge, W. Qiao, L. Zhang, Y. L. Zuo, S. M. Yan, *Appl. Phys. Lett.*, 2009, **94**, 152511.

[50] M. S. Seehra, S. Suri, V. Singh, *J. Appl. Phys.*, 2012, **111**, 07B516.

[51] C. X. Li, P. A. Ma, P. P. Yang, Z. H. Xu, G. G. Li, D. M. Yang, C. Peng, J. Lin, *CrystEngComm*, 2011, **13**, 1003.

[52] J. M. D. Coey, *Solid State Sci.*, 2005, **7**, 660.

[53] Z. L. Yang, D. Q. Gao, Z. H. Zhu, J. Zhang, Z. H. Shi, Z. P. Zhang, D. S. Xue, *Nanoscale Res. Lett.*, 2013, **8**, 17.

[54] T. D. Nguyen, D. Mrabet, T. O. Do, *J. Phys. Chem. C*, 2008, **112**, 15226.

RSC Advances Accepted Manuscript

Figure Caption

Fig. 1 XRD pattern of the $La(OH)_3$ nanowires.

Fig. 2 Electron microscopy analysis of the $La(OH)_3$ nanowires: (a) SEM image, (b) BF-TEM image, (c) HAADF-STEM image, (d) SAED pattern of the area A marked by red false-circle in (b), (e) lattice-resolution HRTEM image of the area B marked by blue square in (b), (f) CBED pattern of the point C marked by green circle in (b), (g) crystal structure model of $La(OH)_3$ and (h) structure model of thee $La(OH)_3$ viewed along *c*-axis direction.

Fig. 3 Element mappings of a single $La(OH)_3$ nanowires: (a) HAADF-STEM image; (b) EDX spectrum; (c) lanthanum mapping; (d) oxygen mapping.

Fig. 4 FTIR spectrum of the $La(OH)_3$ nanowires.

Fig. 5 Magnetic hysteresis loops of the $La(OH)_3$ nanowires measured at room temperature.

Fig. 6 ZFC-FC curve of the $La(OH)_3$ nanowires measured at 10-300 K with an applied magnetic field of 100 Oe.

Fig. 7 M-T curve of the $La(OH)_3$ nanowires measured at 10-300 K with an applied magnetic field of 1000 Oe.

Fig. 8 ESR spectrum of the $La(OH)_3$ nanowires measured at room temperature.

Fig. 9 TEM images of the $La(OH)_3$ nanowires synthesized at different reaction time: (a) 5, (b) 10, (c) 20 and (d) 40 h. Side: distribution statistical histograms of average diameters and lengths for $La(OH)_3$ nanowires, respectively.

Fig. 10 TEM images of the $La(OH)_3$ nanowires synthesized under different volume of

RSC Advances Accepted Manuscript

the solvent (H_2O/ethanol, ml): (a) 30/0, (b) 20/10, (c) 10/20, (d) 0/30. Side: distribution statistical histograms of average diameters and lengths for $La(OH)_3$ nanowires, respectively.

Fig. 11 The synthetic scheme of the formation mechanism for the $La(OH)_3$ nanowires in different experimental conditions.

RSC Advances Accepted Manuscript

Fig. 1

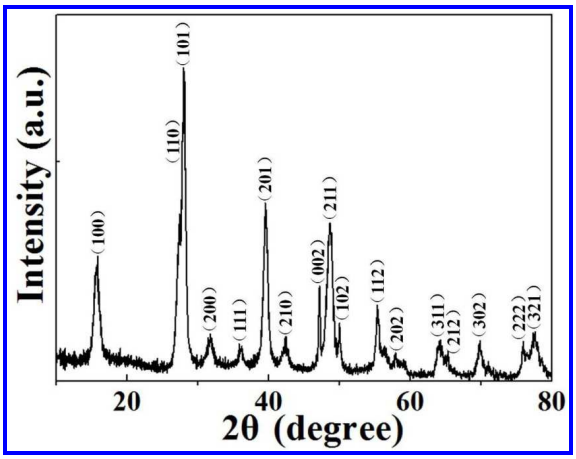

RSC Advances Accepted Manuscript

Fig. 2

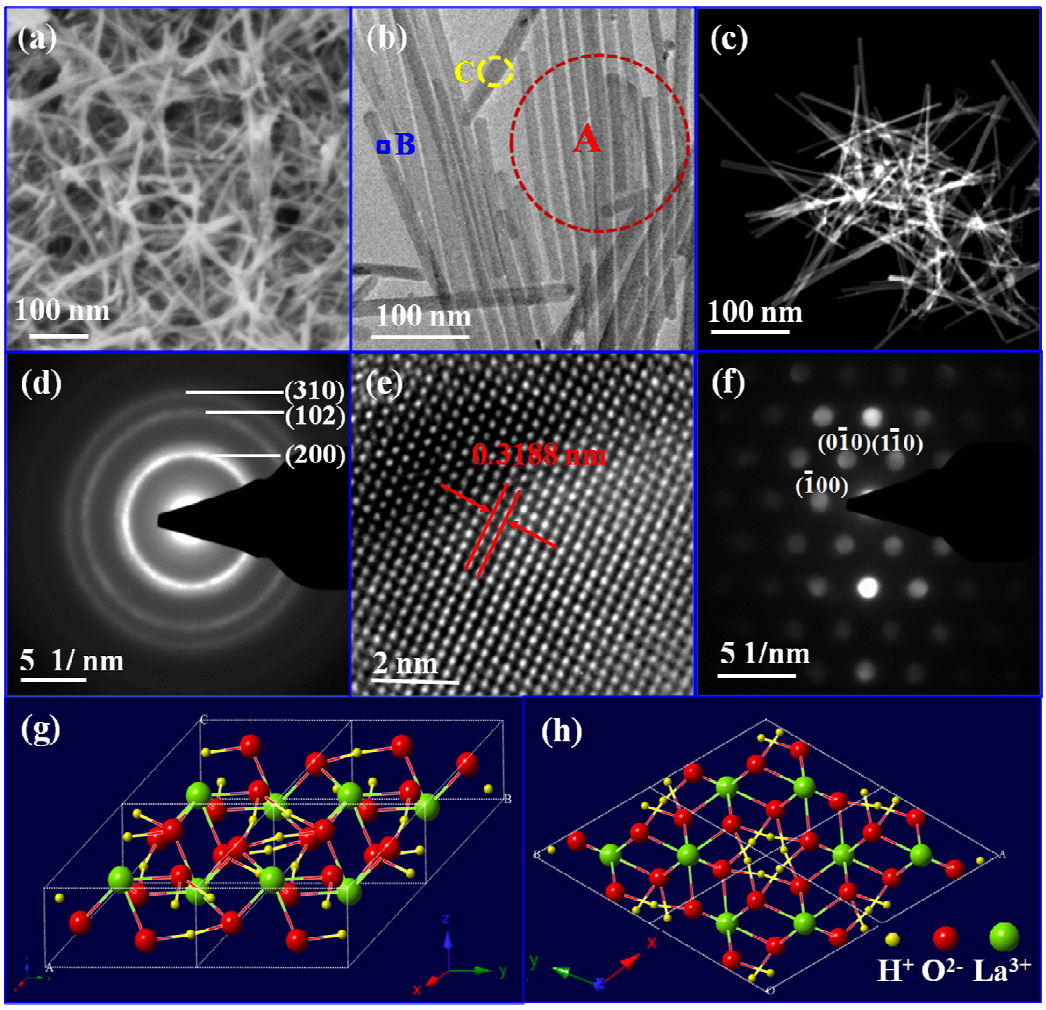

RSC Advances Accepted Manuscript

Fig. 3

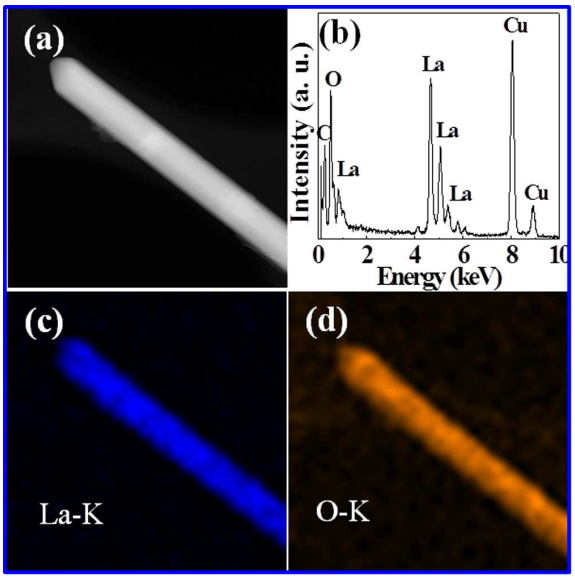

RSC Advances Accepted Manuscript

Fig. 4

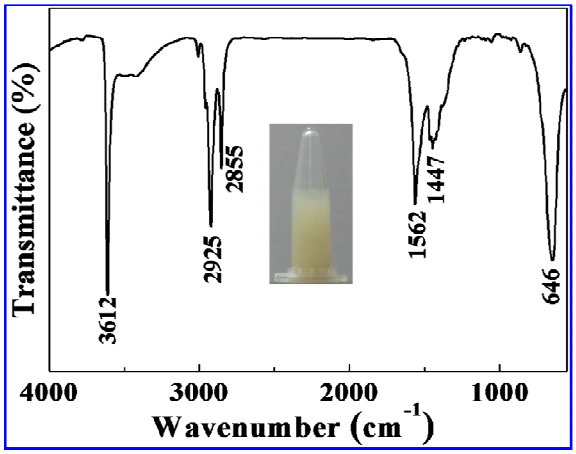

RSC Advances Accepted Manuscript

Fig. 5

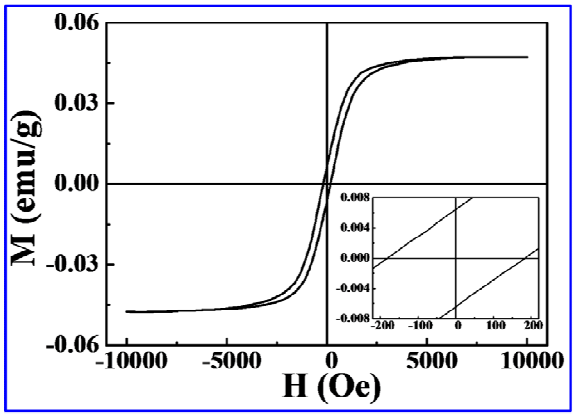

RSC Advances Accepted Manuscript

Fig. 6

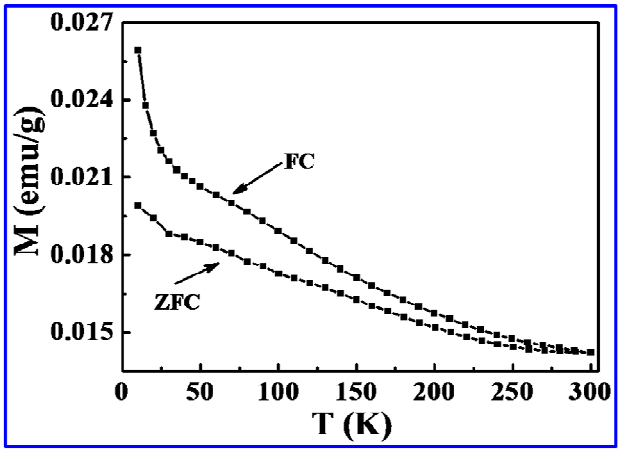

RSC Advances Accepted Manuscript

Fig. 7

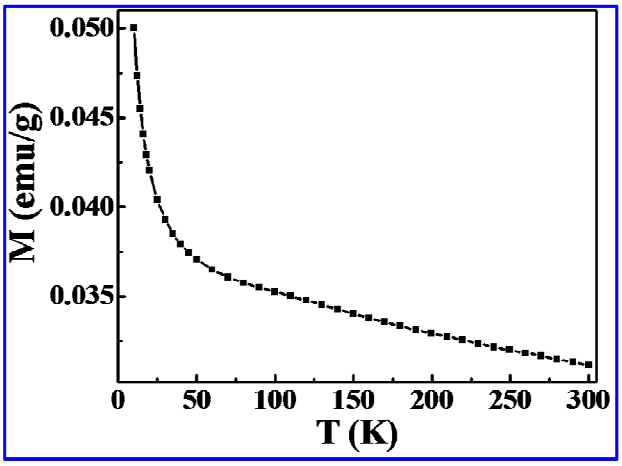

RSC Advances Accepted Manuscript

Fig. 8

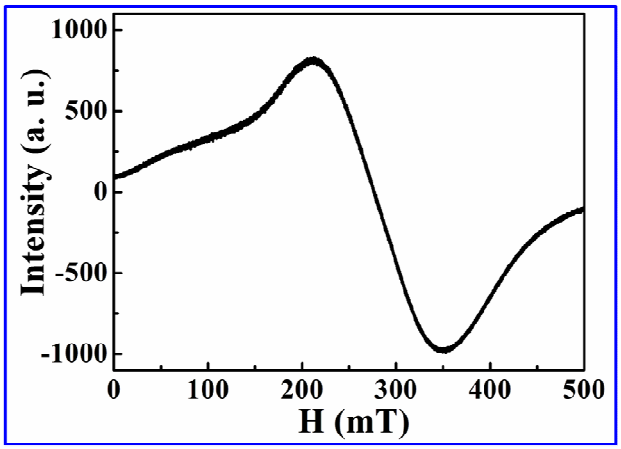

RSC Advances Accepted Manuscript

Fig. 9

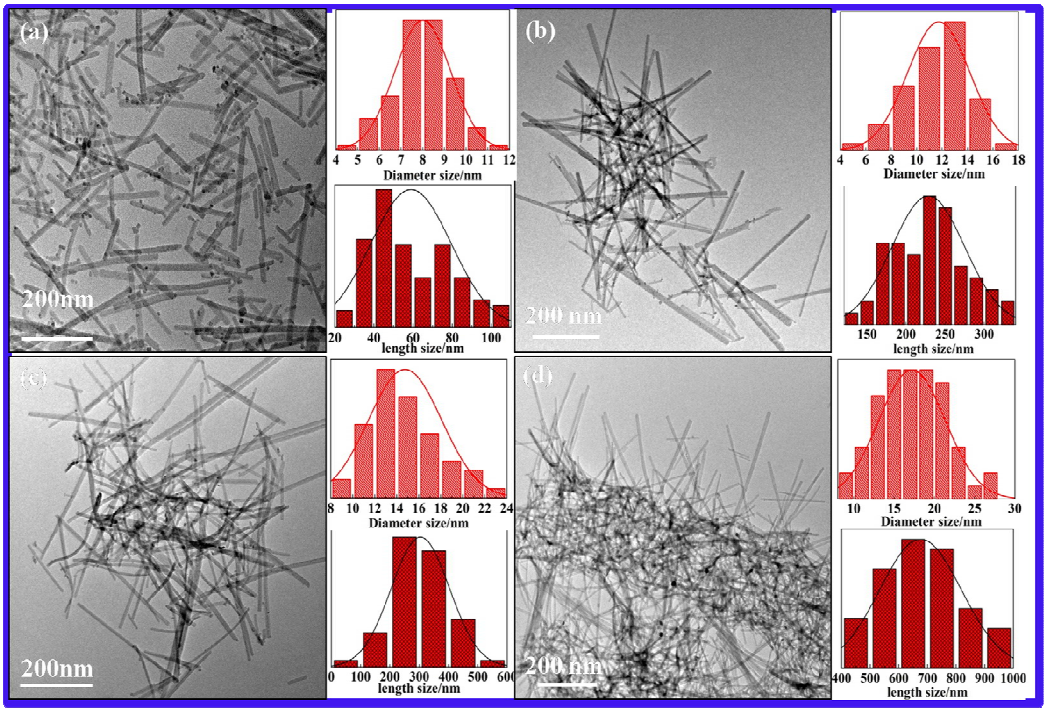

RSC Advances Accepted Manuscript

Fig. 10

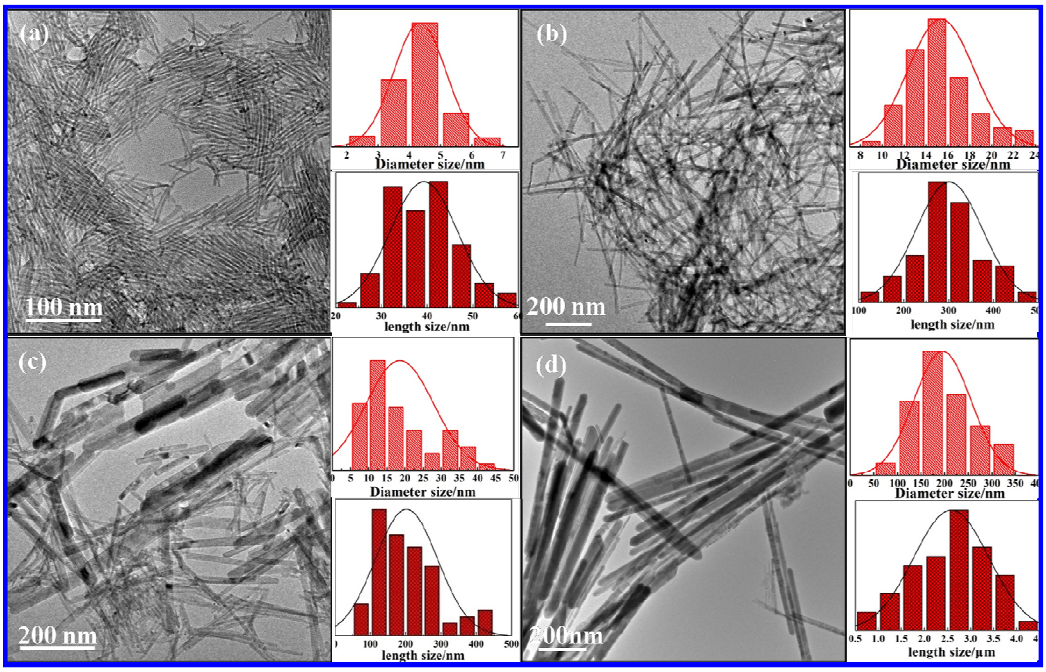

RSC Advances Accepted Manuscript

Fig. 11

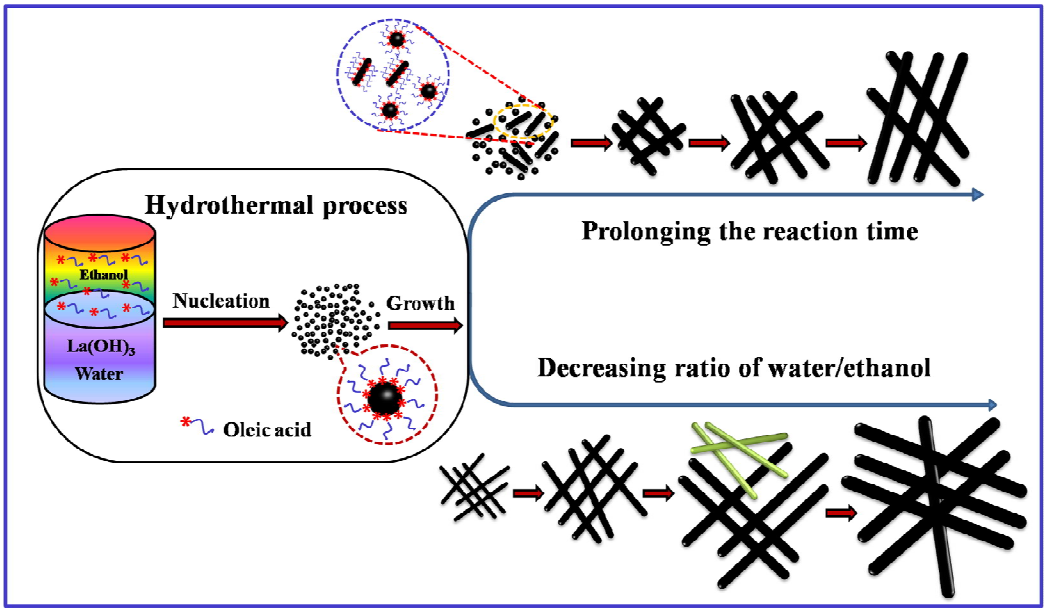

RSC Advances Accepted Manuscript

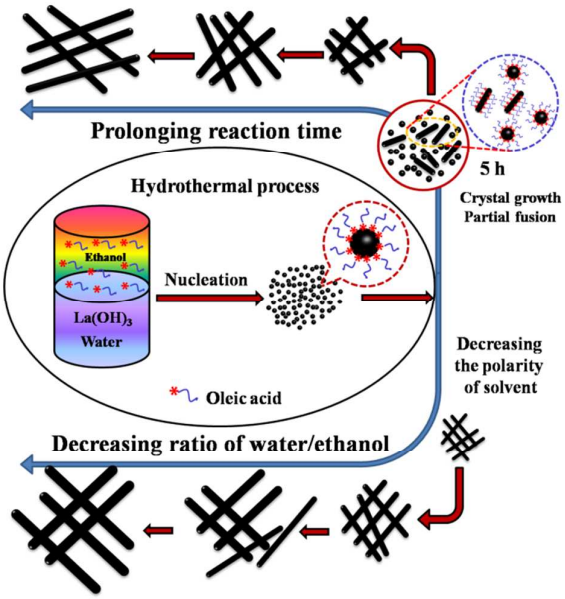

RSC Advances Accepted Manuscript